From plasmon-enhanced molecular spectroscopy to plasmon-mediated chemical reactions

*Chao Zhan, Xue-Jiao Chen, Jun Yi, Jian-Feng Li, De-Yin Wu and Zhong-Qun Tian**

Abstract | The excitation of surface plasmons (SPs) — collective oscillation of conduction-band electrons in nanostructures — can afford photon, electron and heat energy redistribution over time and space. Making use of this ability, plasmon-enhanced molecular spectroscopy (PEMS) techniques with ultra-high sensitivity and surface selectivity have attracted much attention and have undergone considerable development over the past four decades. Recently, the development of plasmon-mediated chemical reactions (PMCRs) has shown the potential to have a large impact on the practice of chemistry. PMCRs exhibit some obvious differences from and potential advantages over traditional thermochemistry, photochemistry and photocatalysis. However, our physicochemical understanding of PMCRs is still far from complete. In this Review, we analyse the similarities and distinctive features of PEMS and PMCRs and compare PMCRs with traditional photochemical and thermochemical reactions. We then discuss how PMCRs can be improved by rationally designing and fabricating plasmonic nanostructures, selecting suitable surface and interface mediators and teaming them synergistically.

Optical diffraction limit
The fundamental maximum of the spatial resolution of an optical system that is due to diffraction.

State Key Laboratory for Physical Chemistry of Solid Surfaces, College of Chemistry and Chemical Engineering, Collaborative Innovation Center of Chemistry for Energy Materials, Xiamen University, Xiamen, China.

**e-mail: zqtian@xmu.edu.cn*

https://doi.org/10.1038/s41570-018-0031-9

Surface plasmons (SPs) are collective oscillating modes of the conduction-band electrons exhibited by certain metals (such as Au, Ag and Cu) and heavily doped semiconductor nanostructures. Because SPs interact effectively with external radiation, they can have notable effects on the optical properties of these materials. For example, localized surface plasmons (LSPs) in nanomaterials can help overcome the optical diffraction limit by concentrating electromagnetic radiation into dimensions smaller than the wavelength of the incident radiation and enable large local field enhancements[1,2]. The field studying the fundamental properties and applications of nanostructure-based SPs is known as nanoplasmonics, which has expanded in the past decade or so from plasmonic physics (including plasmon-enhanced molecular spectroscopy (PEMS), sensing, plasmon heating and wave guiding) to embrace plasmon-mediated chemical reactions (PMCRs) and general plasmon-induced chemical phenomena[3–19].

The distinction between plasmonic physics and plasmonic chemistry cannot be strictly defined. Plasmonic physics includes PEMS techniques such as plasmon-enhanced Raman, infrared and fluorescence spectroscopies, which have been studied since the mid-1970s[3,4]. The idea of using SPs to enhance chemical reactions was first proposed in 1981 and experimentally realized 2 years later[20,21]. At the time of writing, over 4,000 publications on PEMS appear annually, in contrast to several hundred publications on PMCRs, which is a reflection of the relative youth and greater complexity of the latter. The mechanisms of PEMS have been widely investigated, especially in the context of plasmon-enhanced Raman spectroscopy (PERS). By contrast, our physicochemical understanding of PMCRs is still far from complete. In this Review, we discuss to what extent the lessons learned on PEMS over the past four decades may enlighten our understanding and development of PMCRs. In the earliest examples, PMCRs were often studied using PERS. For example, enhanced or accelerated photochemical processes can be tracked using the time evolution of PERS of the reaction products when they are excited by the same wavelength that induced the (enhanced) photochemistry[22]. In such experiments, the nanostructure-based plasmonic enhancement was exploited in two ways: to enable a strong photochemical response and to measure over time the concentration of the products, often produced in meagre quantities[23–26].

Although intimately related, PEMS and PMCRs also differ in crucial ways. Usually, there are more challenges in PMCRs than in PEMS because of the molecular transformation involved in the former. For example, better detection sensitivity is achieved in PEMS measurements when the probed molecules are bound to the plasmonic metal surface. However, the strong bonding and/or adsorption of reactants, intermediates and/or

products to the plasmonic metal surfaces may block the active sites for PMCRs[27,28]. In addition, to verify which reactions SPs can mediate, it is important to fully understand the unique features of PMCRs and explore how to efficiently advance the plasmonic-powered chemical process.

The growth and future of PMCRs crucially depend on the fundamental understanding of the properties of SPs and how they enable chemical reactions. In the first section of this Review, we discuss the basics of SPs, PEMS and PMCRs and how these processes function under varying conditions, from the bare plasmonic nanostructure to the plasmonic nanostructure interacting with molecules and other materials undergoing (or not undergoing) chemical reactions. As most of the current work on PMCRs was carried out on nanostructures, we focus here on LSPs. The discussion of PEMS is focussed on Raman spectroscopy (for example, PERS) because of its pivotal role in the history of PEMS development and its large contributions to the study of PMCRs. In addition, we discuss the scientific intent and advantages of plasmonic chemistry over thermochemistry, photochemistry and photocatalysis. Next, we provide a description of various factors that greatly affect PMCRs, followed by the correlation of PEMS and PMCRs. In the final section, we discuss possible strategies for improving reaction efficiency and selectivity as well as other opportunities in plasmonic chemistry. Throughout this Review, we attempt to clarify the special characteristics of PMCRs by comparing them to PEMS and to other reaction systems, hopefully resulting in a relatively complete current description of PMCRs.

Nanostructure-based surface plasmons

The excitation of SPs

Most plasmonic substrates are based on coinage metals (Au, Ag or Cu) because such metallic nanostructures can support intense SPs with resonances in or near the visible portion of the spectrum, with important consequences for the development of new technologies powered by sunlight. SPs are normally classified as LSPs (BOX 1), in which electrons coherently oscillate locally within and in the vicinity of a nanostructure, and propagating SPs, known as surface plasmon polaritons (SPPs), in which the coherent electron oscillation propagates as a longitudinal wave along the metal surface. When SPs are resonantly excited, they can concentrate the incident light into narrow areas around the nanostructure, which results in electromagnetic near-field enhancement (BOX 1; FIG. 1). The plasmonic structure collects photons over a region larger than its physical size (as an antenna does) and concentrates that energy in a much smaller volume[29–32].

FIGURE 1 shows the local field distribution and extinction spectra of some typical plasmonic Au nanostructures. The electromagnetic field near the metal surface (FIG. 1a) is redistributed at the nanoscale (FIG. 1b,c). Furthermore, when the nanoparticle is at a nanometric distance from a surface (for example, a silicon surface, which is a semiconductor and commonly used to construct heterostructures for a number of technological applications; FIG. 1d,e) and/or another nanoparticle (FIG. 1e,f), the strength of the local electromagnetic field at thus-formed interfaces can be greatly and controllably enhanced. These characteristics are essential for the wide application of PEMS and PMCRs.

The relaxation of surface plasmons

To easily understand the excitation and relaxation of SPs in time, we consider the case of a single nanosphere (FIG. 2). Once excited, SPs in the nanostructure can be relaxed via the re-emission of photons or non-radiative paths[33], depending on the radiance of the plasmon mode[34]. The relaxation process can be separated into several components occurring at different timescales[35–40]. In the first 1–100 fs, the SPs dephase, and excited electron–hole pairs are produced by Landau damping and other photon–electron interactions. The energies of the thus-formed excited electrons range from the Fermi energy E_F to $E_F + \hbar\omega_0$ (where $\hbar = h/2\pi$, h is Planck's constant and ω_0 is the incident light frequency), and those of the corresponding holes range from $E_F - \hbar\omega_0$ to E_F (REF.[36]). During this short period, the excited electron–hole pairs described by a highly non-thermal distribution decay either through the re-emission of photons or the multiplication of carriers via electron–electron interactions. That is, the photonic energy is converted into electronic energy in this process. Thereafter, on a timescale from 100 fs to several picoseconds, the excited carriers transfer their energy to lower-energy electrons through electron–electron interactions, so that the final electron energy assumes a quasi-Fermi–Dirac distribution, as shown in FIG. 2b. Finally, the electron–hole pairs relax, releasing thermal energy through electron–photon interactions on a relatively long timescale, up to hundreds of picoseconds to nanoseconds (FIG. 2c). Accordingly, the effects induced by the excitation and relaxation of SPs can be favourably listed as electromagnetic near-field enhancement, charge-carrier excitation and local heating effects. These effects differ in time, space and energy scales; however, they are all closely related in both PEMS and PMCRs.

Plasmon-enhanced molecular spectroscopy

PEMS are spectroscopic techniques involving SPs excited by light, including linear and nonlinear processes of molecular absorption, scattering and emission, which leads to a large family of techniques including plasmon-enhanced infrared spectroscopy (PEIRS)[41–43], PERS[11,44–48] and plasmon-enhanced fluorescence spectroscopy (PEF)[12,49]. The enhancement factors due to SPs can be expressed as $(|\boldsymbol{E}_{Loc}|/|\boldsymbol{E}_0|)^2$ for PEIRS[50], $(|\boldsymbol{E}_{Loc}|/|\boldsymbol{E}_0|)^4$ for PERS[51] and $(|\boldsymbol{E}_{Loc}|/|\boldsymbol{E}_0|)^2\eta$ for PEF (where $\eta \leq 1$ refers to the emission efficiency and $|\boldsymbol{E}_{Loc}|$ and $|\boldsymbol{E}_0|$ are the amplitudes of the local and incident electromagnetic fields, respectively)[52]. As PERS has been the most studied and applied spectroscopic technique in the PEMS family, we use it to elucidate how plasmonic nanostructures interact with light and molecules in PEMS. For historical development[53], landmark methods[47,48,54] and the applications of PERS[22,48,55,56], we refer readers to the reviews and book chapters cited in this sentence. In this section, molecules adsorbed on plasmonic nanostructures do not undergo chemical reactions, as shown in the top left of FIG. 3, and we later elucidate any link between PEMS and PMCR.

Landau damping
The damping effect of longitudinal space charge waves in plasma or a similar environment. Landau damping occurs because of the energy exchange between an electromagnetic wave and particles (for example, electrons) in the plasma, which can interact strongly with the wave. In a surface plasmon system, the Landau damping process represents the direct absorption of a photon assisted by the surface plasmon momentum, creating a hot hole and a hot electron.

Fermi–Dirac distribution
The distribution of particles over energy states in systems consisting of many identical particles that obey the Pauli exclusion principle.

Electrostatic approximation
The assumption that the phase of the harmonically oscillating electromagnetic field is practically constant over the particle volume, so that one can calculate the spatial field distribution by assuming the simplified problem of a particle in an electrostatic field.

Drude model
A model used to explain the transport properties of electrons in materials in which the microscopic behaviour of electrons in a solid is treated classically. It is the basic model used in the study of optical properties of different materials and is commonly used to explain the dielectric function of plasmonic nanostructures.

Electromagnetic enhancement mechanism of PERS

Raman scattering provides information on molecular vibrational modes with high spectral resolution (about 1 cm^{-1}) over a wide spectral window (5–4,000 cm^{-1}). However, the Raman scattering cross section is normally small, typically 10^6 and 10^{14} times smaller than that of infrared and fluorescence, respectively[53]. In the case of PERS, plasmonic nanostructures increase the effective Raman cross section, allowing even the Raman spectra of single molecules to be detected[57–60] (FIG. 3a). This is primarily due to the enhancement of the electromagnetic near-field in the vicinity of the nanostructure as a consequence of SP excitation (FIG. 2a). This effect is often referred to as electromagnetic PERS enhancement (BOX. 2)[5,8,61–64].

This electromagnetic enhancement effect is characterized by surface specificity and geometry inhomogeneity. Surface specificity results from the dependence of $|\boldsymbol{E}_{Loc}|$ on surface distance, which is proportional to D^{-3} (where D is the distance of the probed molecule from the SP dipole centre) and results in the enhancement factor for PERS being proportional to D^{-12} (REF.[31]). This means that the Raman spectra of molecules in close proximity to the plasmonic surface can be greatly enhanced compared with molecules residing in the surrounding media (FIG. 3a). The geometric inhomogeneity is a consequence of the spatial localization of the enhanced electromagnetic near-field[52], determined by the structure and morphology of the plasmonic nanostructure as well as the polarization of the incident light. Usually, electromagnetic enhancement factors are higher at the sharp curvature edges, tips and nano-interspaces between coupled particles. Highly localized regions on a PERS-active surface with extraordinarily large enhancement factors are the so-called hot spots, which contribute to most of the PERS signal[52,56]. However, the probability of hot spots is much lower than that of the medium-enhanced or non-enhanced regions (FIG. 1f).

Chemical enhancement mechanism of PERS

The total enhancement of the spectroscopic signal primarily results from SPs; however, other non-electromagnetic effects, including chemical enhancement and charge transfer, can contribute to the total enhancement, and their contributions vary from molecule to molecule[6,51,65]. In these cases, the probed molecule interacts strongly with the plasmonic nanostructure in processes that involve molecular rearrangement, surface binding, chemical adsorption and/or formation of surface complexes. Because chemical enhancement is accompanied by charge transfer, it is also known as charge transfer enhancement.

Charge transfer can proceed either directly from the molecule towards the plasmonic nanostructure and vice versa or indirectly, mediated by other surface species such as co-adsorbates, solvent molecules or electrolyte ions. It is therefore necessary to consider three types of charge transfer processes[66]. The direct mechanism involves charge transfer between the probed molecule and the surface in either direction, which changes the electronic state population of the probed molecule and thus its polarizability, leading to an increase or decrease in the Raman scattering signal. A strong charge transfer mechanism can arise from the formation of surface complexes including the partially charged metal surface atom, the probed molecule and/or the co-adsorbed surface species. Some surface complexes can also form as new molecules that have new electronic transitions in resonance with the incident light, resulting in a resonant Raman process. Charge transfer can also be photoinduced[66,67], as observed in some electrochemical Raman spectroscopy experiments (FIG. 3b). The applied potential can continuously tune the Fermi level of the plasmonic nanostructure. When the energy of the incident photon matches the energy difference between the orbitals of the adsorbed molecules and the Fermi level of the metal or between the potential-independent charge transfer state and the potential-dependent ground state of the surface complex (FIG. 3b, top right), a resonance-like Raman scattering process is promoted, in which the amplified Raman intensity reaches a maximum at specific potential

Box 1 | **The basics of localized surface plasmons**

Localized surface plasmons are non-propagating excitations of conduction-band electrons of metallic nanostructures coupled to an electromagnetic field[32]. In a simple model, if a homogeneous metallic sphere of radius (r) is much smaller than the wavelength of the incident light (λ), the electrostatic approximation can be applied to evaluate the induced dipole ($\boldsymbol{P}_M$) of the metallic sphere under irradiation. $\boldsymbol{p}_M$ is proportional to the incident electromagnetic field ($\boldsymbol{E}_0$) according to the following equation:

$$\boldsymbol{p}_M = 4\pi\varepsilon_0\varepsilon_m r^3 \frac{\varepsilon_M(\omega)-\varepsilon_m}{\varepsilon_M(\omega)+2\varepsilon_m}\boldsymbol{E}_0$$

where ε_0, ε_m and $\varepsilon_M(\omega)$ correspond to the permittivity of the vacuum, the permittivity of the surrounding environment and the dielectric function of the metal sphere, respectively. The induced dipole can also be expressed in terms of the polarizability of the metal sphere (α_M), as $\boldsymbol{p}_M = \varepsilon_0\varepsilon_m\alpha_M\boldsymbol{E}_0$; therefore, α_M can be defined as:

$$\alpha_M = 4\pi r^3 \frac{\varepsilon_M(\omega)-\varepsilon_m}{\varepsilon_M(\omega)+2\varepsilon_m}$$

Equation 2 tells us that the polarizability of the small metallic sphere with a sub-wavelength diameter experiences a resonant enhancement when $\varepsilon_M(\omega)+2\varepsilon_m$ tends to 0. Based on the classic Drude model, $\varepsilon_M(\omega)$ is a complex term whose real ($\mathrm{Re}[\varepsilon_M(\omega)]$) and imaginary ($\mathrm{Im}[\varepsilon_M(\omega)]$) parts can be estimated as a function of the frequency of the excitation line, the plasma frequency of the bulky metal and the collision frequency of the free electron gas[32]. Therefore, localized surface plasmon resonance (LSPR) can be excited if $\mathrm{Re}[\varepsilon_M(\omega)]$ is negative and close to $-2\varepsilon_m$ and $\mathrm{Im}[\varepsilon_M(\omega)]$ is positive but small. For the coinage metals, the resonance condition is satisfied under visible-light excitation, resulting in their wide application in plasmon-enhanced molecular spectroscopy (PEMS) and plasmon-mediated chemical reactions (PMCRs).

The distributions of the induced local electromagnetic fields inside ($\boldsymbol{E}_{In}$) and outside ($\boldsymbol{E}_{Out}$, also known as $\boldsymbol{E}_{Loc}$) of the metallic sphere can then be evaluated as:

$$\boldsymbol{E}_{In} = \frac{3\varepsilon_m}{\varepsilon_M(\omega)+2\varepsilon_m}\boldsymbol{E}_0$$

$$\boldsymbol{E}_{Out} = \boldsymbol{E}_0 + \frac{(3n^2-1)\boldsymbol{p}_M}{4\pi\varepsilon_0\varepsilon_m}\frac{1}{D^3}$$

Here, $\boldsymbol{n}$ is the unit direction vector and D is the distance from the sphere centre. The enhanced local electric field of the plasmonic nanostructure is roughly proportional to $1/D^3$ and results in the surface specificity of PEMS and PMCRs. The resonance in α_M implies an enhancement of the local electromagnetic field. It is this field enhancement at the plasmon resonance on which PEMS and PMCR rely.

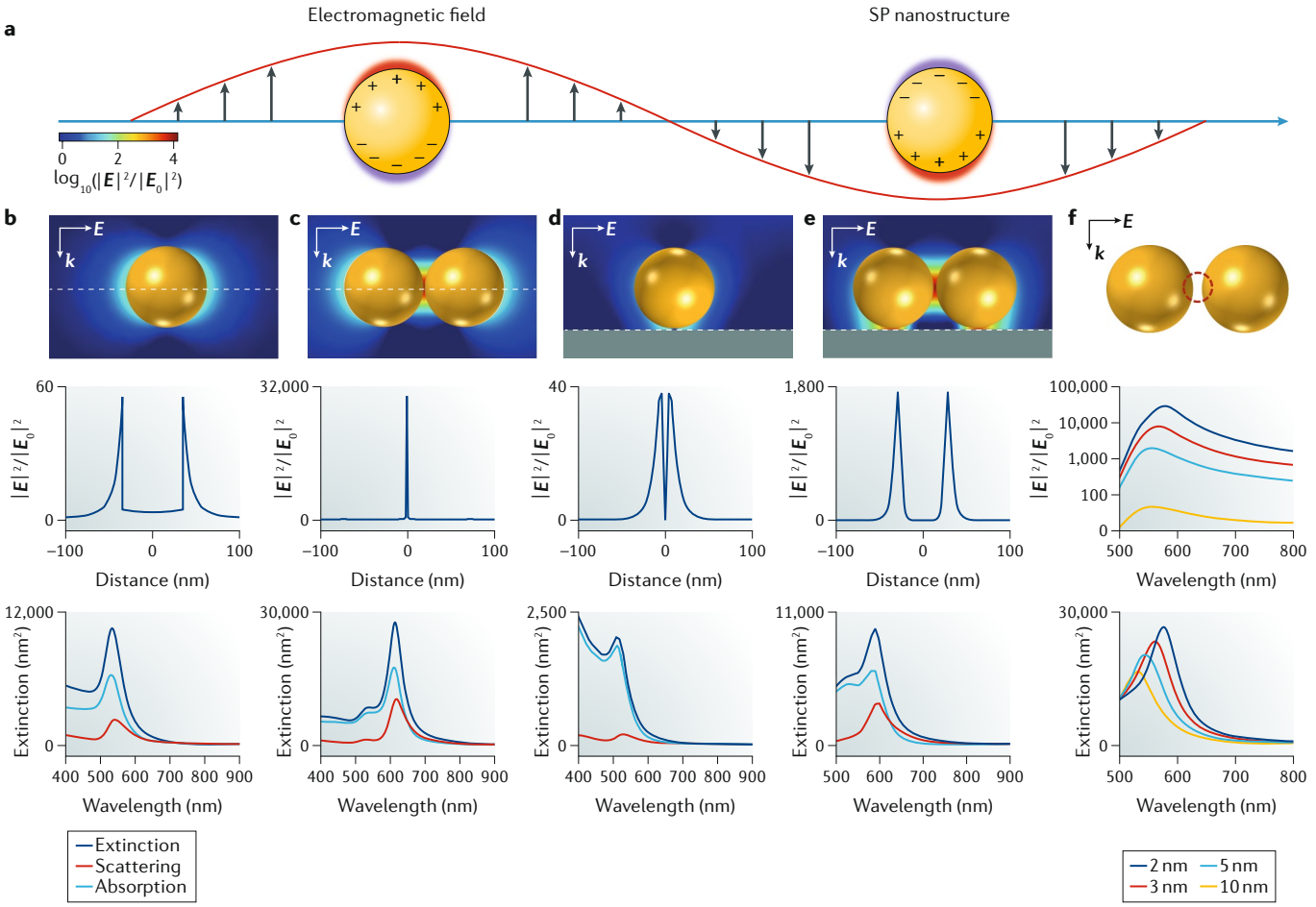

Fig. 1 | **Surface plasmon excitation, optical confinement and spectral features of some typical nanostructures.** **a** | Collective oscillation of conduction-band electrons in a nanostructure induced by incident light. **b**–**e** | Electromagnetic field distributions (second and third rows) and extinction spectra (fourth row) of some typical Au nanostructures computed using finite-element simulations, where ***E*** is the electromagnetic field and ***k*** is the wave vector of incident light. **b** | An isolated Au nanosphere of 60 nm diameter in vacuum. **c** | A nanosphere dimer with a gap size of 2 nm in vacuum. **d** | A single Au nanosphere at 1 nm distance from a flat Si surface. **e** | The Au nanosphere dimer (gap of 2 nm) at 1 nm distance from a Si surface. The enhanced local electromagnetic field is expressed by $|\boldsymbol{E}|^2/|\boldsymbol{E}_0|^2$, where $|\boldsymbol{E}|^2$ and $|\boldsymbol{E}_0|^2$ are the amplitude of the local and the incident electromagnetic field, respectively. The white dashed lines drawn in the second row indicate the direction along which the local electromagnetic fields are enhanced, as depicted in the third row. The excitation lines from part **b** to part **e** are 550 nm, 640 nm, 550 nm and 600 nm, respectively, which locate around the resonance peak shown in each extinction spectrum in the bottom row. **f** | The local field enhancement at the mid-point of the nanogap and the extinction spectra of the Au nanosphere dimer with various gap sizes ranging from 2 nm to 10 nm. SP, surface plasmon.

energies (for example, E_2 shown in FIG. 3b, bottom). As the incident light frequency (ω_0) varies, different applied potentials are needed to ensure resonance with the charge transfer states.

In general, enhancement through either the electromagnetic or charge transfer mechanism can be explained by the increased probability of the Raman scattering process, as illustrated in FIG. 3. The enhancement of the electromagnetic field around the plasmonic nanostructure results in an increase in the electron transition between the electronic ground state and the virtual intermediate state. Whereas charge transfer enhancement (strong and photoinduced charge transfer) increases the probability of resonance-like transitions between the electronic real states. Accordingly, the spatial aspect is distinctively different for these two mechanisms: the electromagnetic mechanism occurs over long-range distances (about 10 nm), whereas the charge transfer mechanism occurs over short-range distances (approximately 1 nm or less).

It is necessary to emphasize that charge transfer enhancement is molecule-specific and dependent on a three-body (molecule, incident photon and plasmonic nanostructure) interaction. All charge transfer processes take place under SP conditions (FIG. 2); therefore, they depend on the strengths of the electromagnetic and thermal fields and the density of the excited carriers. More precisely, charge transfer processes should be called SP-based charge transfer processes. Moreover, charge transfer and electromagnetic enhancement can interact and influence each other, such that especially strong and photoinduced charge transfer mechanisms are improved by electromagnetic enhancement, while charge transfer can change the properties of the SPs that determine the

Fermi level
The highest energy level that an electron can fill in the solid state at absolute zero temperature.

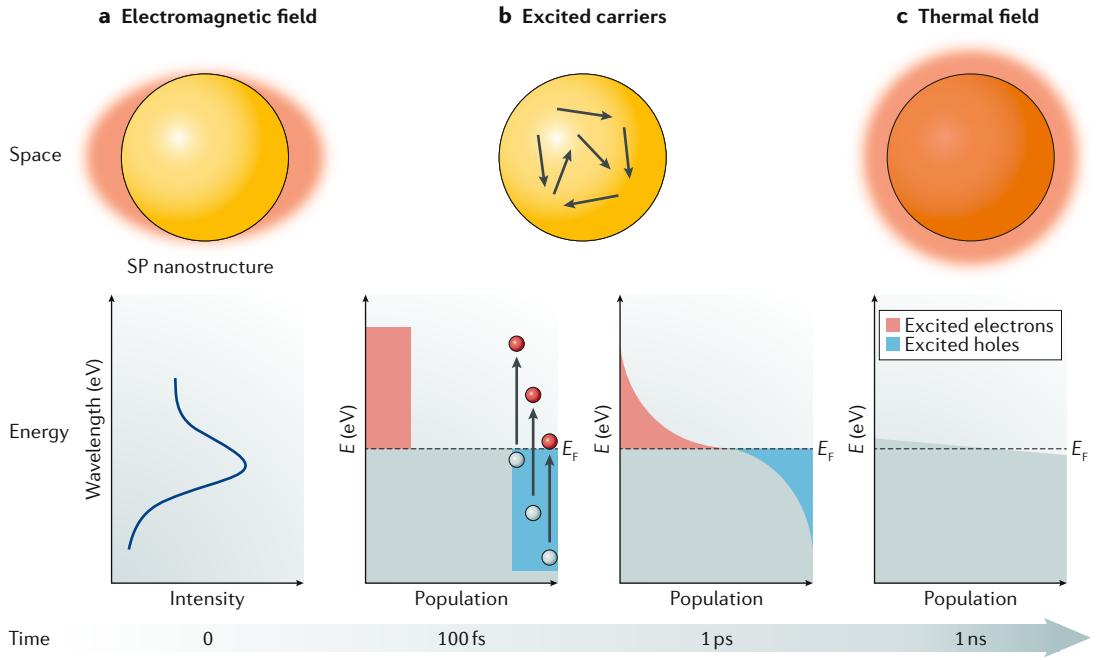

Fig. 2 | **Three main effects induced by the excitation and relaxation of surface plasmons.** The three main effects induced by the excitation and relaxation of surface plasmons (SPs) are the electromagnetic field enhancement, charge-carrier excitation and thermal effect. A SP nanoparticle illuminated by a laser pulse is used as an example. The schematic diagrams show their characteristics in space, energy and time. **a** | The redirection of incident light by the excitation of SPs leads to an electromagnetic near-field enhancement characterized by a specific resonance wavelength for a specific nanostructure. **b** | Formation and relaxation of the excited carriers. Incident photons induce changes in the population of the electronic states, which are followed by the energy redistribution of excited carriers over different timescales. The red areas above the Fermi energy (E_F) represent the distributions of excited electrons, and the blue areas below E_F represent the excited hole distributions (the arrows represent electron–electron interactions). **c** | The electronic energy converts into thermal energy, which leads to local heating. Energy (E) is expressed in eV. Part **b** is adapted with permission from REF.[35], American Chemical Society, and REF.[40], Springer Nature Limited.

electromagnetic strength[68]. For a comprehensive understanding of PEMS, PMCRs and their relationship, great attention needs to be paid to these important and correlated phenomena. It is clear that the SP-based charge transfer process overlaps PMCRs to some extent, for example, when probing a molecule or when a molecule is undergoing a chemical reaction.

Plasmon-mediated chemical reactions

According to the basic processes of SP excitation and relaxation (FIG. 2), our aim is to compare PMCRs with three types of relevant reaction systems and establish a new and integrated description for PMCRs that takes into account time, space, energy and probability (FIG. 4). It is important to note that different types of SP effects usually occur simultaneously, and the excitation and relaxation properties of SPs can be influenced by the molecules adsorbed on the surface. Based on a careful comparison, we elaborate the specific characteristics and physicochemical descriptions of PMCRs that differentiate them from other, better-understood reactions.

Electromagnetic field-mediated reactions

As in traditional photochemistry, electromagnetic near-field-mediated photochemistry is associated with electronic excitation of the reactant molecules[69–74] (FIG. 4a). The enhanced electromagnetic near-field enables a dramatic increase in light absorption owing to increased light intensity and/or extended light paths, which results in an increased excitation probability of the reactant or substrate, such as a semiconductor[75] (FIG. 5Aa). For example, the enhanced electromagnetic near-field generated upon visible-light illumination of Au nanoparticles loaded on the surface of a N-doped TiO_2 (as efficient absorber of visible light) electrode was demonstrated to lead to a 66-fold increase in the photocurrent of water splitting, whereas a 4-fold reduction in the photocurrent was observed under ultraviolet-light illumination[76]. In another similar system, in which Ag nanoparticles were incorporated into a N-doped TiO_2 photoanode, the increase in the photocurrent was attributed to the enhancement of the electromagnetic field at the interface between the Ag nanoparticles and the N-doped TiO_2 photoanode and corroborated by the dependence of the photocurrent on the light intensity[77]. The enhanced electromagnetic near-field also enables the control of photochemical reactions in small volumes, even on the nanometric scale. For example, the two-photon polymerization of the epoxy-based negative photoresist (SU8) was investigated on gold nanoblocks separated by 6 nm gaps (FIG. 5Ab). By changing the polarization of the light, the reaction proceeded at different positions on the nanoblocks (substrate), in agreement with finite-difference time-domain predictions of the near-field stength[78]. Moreover, electromagnetic enhancement allowed nonlinear photoexcitation to be achieved in these experiments, even under low-intensity

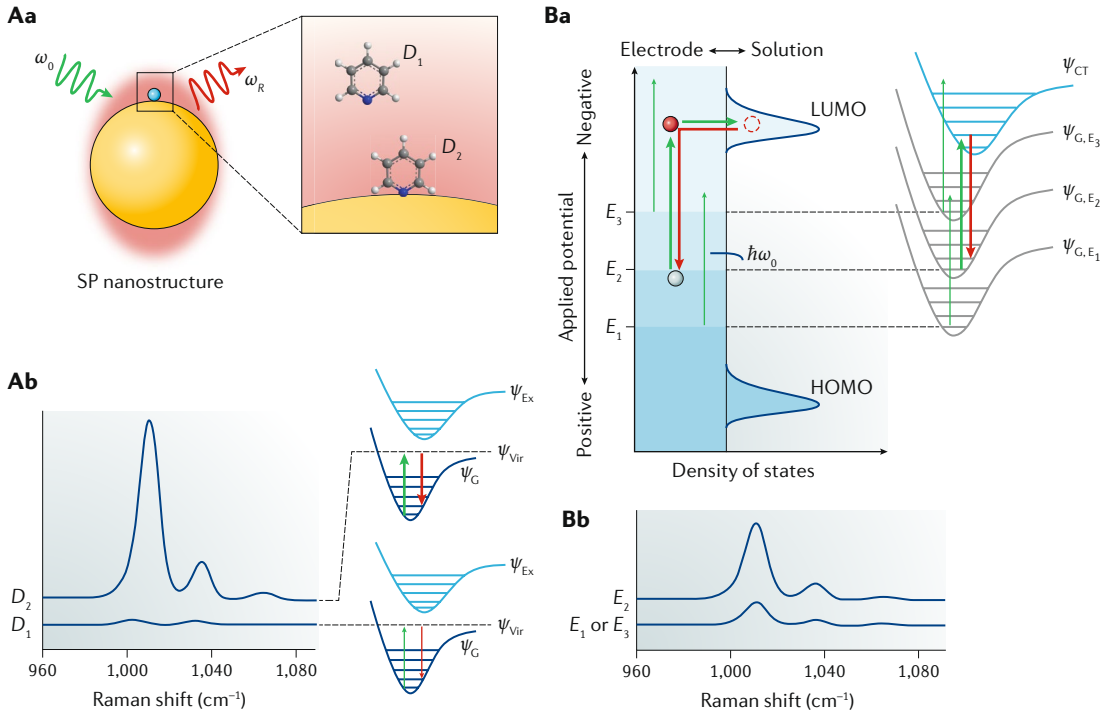

Fig. 3 | **The plasmon-enhanced Raman scattering process. A** | The Raman scattering process is predominantly promoted by the electromagnetic near-field enhancement experienced by the probed molecule near the plasmonic nanostructure. The plasmonic nanostructure acts as the optical antenna that amplifies the energy of incident radiation of frequency ω_0 and transmits it with a new frequency ω_R as a result of recombination processes (part **Aa**). The intensity of the vibrational bands is proportional to the fourth power of the local field strength ($|\boldsymbol{E}_{Loc}|^4$) and the local field strength is inversely proportional to the third power of the distance from the plasmonic nanostructure (D^{-3}). In total, the intensity of plasmon-enhanced Raman scattering (PERS) bands is determined by the probability of the Raman scattering transition: the larger the local field strength and the closer the probed molecule to the plasmonic nanostructure, the higher the probability of Raman scattering (part **Ab**). **B** | Charge transfer (CT) can occur if the probed molecule interacts strongly with the plasmonic substrate and if the molecule energy levels and the Fermi level of the metal are in resonance with the exciting light. A resonant-like Raman scattering process through photon-induced CT is illustrated at the electrode–solution interface where the Fermi level of the plasmonic substrate can be easily tuned by the electrode potential to be in resonance with the incident photon energy $\hbar\omega_0$ (part **Ba**, left). The corresponding probability of the energy state transition is maximized when applied at the resonant potential E_2 and is decreased at the off-resonant potentials E_1 and E_3 (part **Ba**, right), resulting in a higher Raman intensity at E_2 state (part **Bb**). ψ_{Ex}, ψ_{Vir} and ψ_G in part **A** denote the energy states of the first excited state, the virtual state and the ground state of the probed molecule, respectively. ψ_{G,E_i} and ψ_{CT} in part **B** denote the potential-dependent ground state and the potential-independent CT state of the surface complex, respectively, where the surface complex is the combination of the electrode outmost layer and the adsorbed probed molecule. HOMO and LUMO are the highest occupied molecular orbital and the lowest unoccupied molecular orbital of the adsorbed molecule, respectively. The green arrows correspond to electronic excitations, and the red arrows correspond to electronic decays, while the thickness of the arrow represents the event probability. SP, surface plasmon.

illumination. However, overlap of the absorption spectra of the plasmonic nanostructure and the reaction precursor is essential to complete a reaction efficiently.

Excited-carrier-mediated photocatalytic reaction

Similar to photocatalytic reactions[79–83] (FIG. 4b), PMCRs are mediated by excited electrons (or holes) induced by SPs that are injected from the plasmonic metal to a neighbouring molecule or into a semiconductor exhibiting suitable energy levels in contact with the plasmonic metal[84]. This reaction mechanism has been proposed to lead to photocurrent enhancement owing to water oxidation observed upon visible-light irradiation of TiO_2 sol gel films incorporating Au or Ag nanoparticles[85]. A similar mechanism was proposed for catalytic oxidation reactions, such as ethylene epoxidation, CO oxidation and NH_3 oxidation (typical exothermic reactions), the efficiencies of which were considerably improved by the irradiation of Ag plasmonic nanostructures with low-intensity visible light. The resulting improvements were attributed to the SP-excited electrons that were transferred to the oxygen molecules, which promoted oxygen activation by forming transient negative-ion states[15,86] (FIG. 5Ba). Water splitting, however, is a typical example of an endothermic reaction and was carried out by SP-excited electrons and holes from Au nanorod arrays in contact with a TiO_2 film upon visible-light irradiation[14] (FIG. 5Bb). These works represent a milestone in PMCR research and inspired many groups to enter this field.

An in situ PERS study revealed that *p*-aminothiophenol (PATP) can be selectively oxidized to *p*,*p*′-dimercaptoazobenzene (DMAB) on Au or Ag nanoparticles at room

Box 2 | **The basics of the electromagnetic enhancement mechanism of PERS**

From a quantum mechanical perspective, the Raman scattering process of a molecule can be divided into two simultaneous steps. One is the absorption of an incident photon ($\hbar\omega_0$) to excite a transition from a low-energy level to an intermediate virtual state, which has no physical reality but is useful in theory modelling[64]. The other is the instantaneous re-emission of a photon with a different energy ($\hbar\omega_R$) through a follow-up electron–hole recombination back to the low-energy level. The energy difference between the incident and scattered photon corresponds to that of a given vibrational mode of the molecule. Raman scattering is an inelastic scattering process. When the scattered photon has less energy than the incident photon, the process is called a Stokes process, which usually has a much higher probability than the anti-Stokes process, in which the scattered photon has a higher energy than the incident photon.

For a given Raman mode of a probed molecule, its dipole moment ($\boldsymbol{p}_0$) is correlated to both the Raman polarizability tensor (α) and the incident electric field ($\boldsymbol{E}_0$), $\boldsymbol{p}_0 = \alpha\boldsymbol{E}_0$. When the probed molecule is in close proximity to a plasmonic nanostructure (FIG. 3a, top left), the resulting oscillating dipole should be rewritten as $\boldsymbol{p} = \alpha\boldsymbol{E}_{Loc}(\omega_0)$. If such a dipole radiates in free space, the corresponding dipolar power, which is proportional to $|\boldsymbol{p}|^2$, would greatly increase by a factor of:

$$M_{Loc}(\omega_0) = \frac{|\boldsymbol{E}_{Loc}(\omega_0)|^2}{|\boldsymbol{E}_0|^2}$$

where $M_{Loc}(\omega_0)$ is typically defined as the local field enhancement factor and produced during excitation of the Raman dipole. Clearly, $M_{Loc}(\omega_0)$ dependents on wavelength and would be maximized when the incident light couples with the localized surface plasmon resonance (LSPR) of the plasmonic nanostructure. Nevertheless, in plasmon-enhanced Raman scattering (PERS), the Raman dipolar radiation is strongly modified by the presence of the plasmonic nanostructure. The total radiation power of the oscillating dipole close to the metal surface (P_{Rad}) can be enhanced by a factor of $M_{Rad} = P_{Rad}/P_0$, where P_0 refers to the power of radiation with the same dipole and the same amplitude in free space. Owing to the difficulty in estimating M_{Rad}, it is often assumed that $M_{Rad}(\omega_R) \approx M_{Loc}(\omega_R)$ (REF.[51]), resulting in:

$$M_{Rad}(\omega_R) = \frac{|\boldsymbol{E}_{Loc}(\omega_R)|^2}{|\boldsymbol{E}_0|^2}$$

$M_{Rad}(\omega_R)$ is the so-called radiation enhancement factor, which is associated with the re-emission step of the Raman process. It depends on the substrate geometry and optical properties, the dipole position, orientation and its emission frequency ω_R. When ω_R couples to the radiative LSPR of the plasmonic nanostructure, the dipole would be forced to radiate more energy[51]. If we consider only the local field (excitation) enhancement and the radiation (re-emission) enhancement, the electromagnetic (EM) enhancement factor G can be approximated to:

$$G \approx M_{Loc}(\omega_0)M_{Rad}(\omega_R) \approx \frac{|\boldsymbol{E}_{Loc}(\omega_0)|^2}{|\boldsymbol{E}_0|^2}\frac{|\boldsymbol{E}_{Loc}(\omega_R)|^2}{|\boldsymbol{E}_0|^2} \approx \frac{|\boldsymbol{E}_{Loc}(\omega_0)|^4}{|\boldsymbol{E}_0|^4}$$

An additional approximation is often made for low-frequency vibrations when ω_R is not very different from ω_0, resulting in the more familiar expression shown above. This is the well-known $|\boldsymbol{E}|^4$ approximation for the PERS enhancement factor[8,56]. For example, when the enhanced field strength is $10^2|\boldsymbol{E}_0|$, the EM enhancement factor G for PERS can reach ~10^8.

temperature by SP-excited carriers[26,87] (FIG. 5Bc). It was also found that SP-excited electrons can induce the six-electron photocatalytic reduction of 4-nitrothiophenol to 4-aminothiophenol on Ag nanostructures in the absence of conventional chemical reducing agents, such as hydride reagents[88]. So far, a number of other chemical reactions have been induced or enhanced under mild conditions, such as normal temperature and pressure, by SP-excited carriers, including H_2 dissociation[89], N_2 dissociation[90], CO_2 reduction[91] and NH_3 synthesis[92], among others[16,93]. It should be emphasized that SP-excited carriers are quite different from excited carries generated in semiconductors or dyes in terms of energy distribution, lifetimes and other features.

Thermochemical reaction

Temperature can greatly affect the reaction rates, as defined by the Arrhenius law (FIG. 4c). Therefore, one can exploit the heat produced by the decay of excited SPs to control a chemical reaction[94,95]. Plasmonic nanostructures can be employed as nanosources of heat to increase chemical reaction rates[96]. This would reduce the demand for other non-renewable energy sources. Specifically, plasmonic nanostructures can convert incident light into heat more efficiently than most other means[13,95]. Furthermore, the presence of SPs can improve the heating dynamics and efficiencies through the confinement of heat in nanometric volumes (confinement effect)[97–99] (FIG. 5c). Normally, it is difficult to localize thermal regions to the nanoscale using traditional means. This makes plasmon-mediated heating unique and promising.

Factors influencing PMCRs

To efficiently power chemical reactions using SPs, one needs to understand the entire system holistically. Three integral components are involved in PMCRs: the SPs, the chemical reaction and the surface or interface on which the reaction takes place. These three components influence PMCRs; however, the various types of PMCRs have unique requirements for these three components.

Factors influencing surface plasmons. All the effects due to SPs, such as electromagnetic near-field enhancement, charge-carrier excitation and the local heating effect, strongly depend on size, material properties, morphology and state of aggregation[95,100,101]. For instance, the properties of SPs strongly depend on the geometry of the plasmonic system. By changing the geometry of the nanoparticle, one can control the light harvesting ability of absorbers over most of the solar spectrum[102]. The SP properties can also be greatly influenced by the aggregation state of the plasmonic structures (FIGS 1f, 5Ca,Cb). For example, it was found that the photocurrent of semiconductors or dyes could be enhanced in the gap between Au nanoparticles and Au films. These gaps are called hot spots and are the locations at which intense enhancements of PEMS occur[103]. Accordingly, different types of PMCRs require the design of specific structures to adjust the SP properties to the specific application. For example, in PEMS, the nanoparticles usually range from 10 nm to 180 nm in diameter. In general, larger particles lead to a higher enhancement in the electromagnetic field. However, in a certain size range, the energy distribution of the excited carriers follows the opposite trend. A theoretical study showed that the production rate and energy distribution of the excited carriers in Ag nanoparticles with diameters varying from 5 nm to 25 nm change with the particle size and the lifetime of the excited carriers: larger nanoparticles and shorter lifetimes result in higher carrier production rates but lower excited carrier energies and vice versa[104].

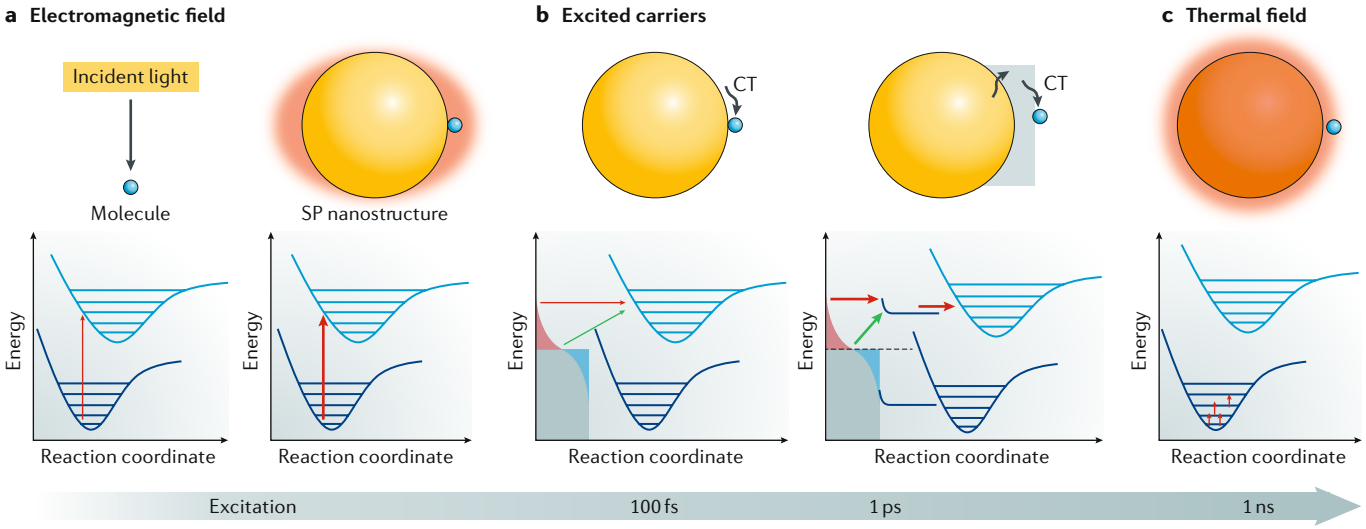

Fig. 4 | **A microscopic view of plasmon-mediated chemical reactions. a** | The left panel shows a common photochemical reaction of a molecule initiated by an electronic excitation from the ground state to an excited state to overcome the activation energy. On the right, electromagnetic near-field enhancement resulting from surface plasmons (SPs) greatly increases the probability of molecular excitation for a molecule near the plasmonic nanostructure. This interaction will increase the rate and/or yield of the photochemical reaction but requires overlap of the absorption spectrum of the plasmonic nanostructure with that of the molecule. In addition, the precursors should be located in the enhanced electromagnetic field. **b** | The left panel shows how SP-excited carriers can transfer to the molecule near the surface through direct or indirect charge transfer (CT) process[18,139] and then mediate the chemical reaction, similar to photocatalysis. In the direct process, SP decay occurs directly by interfacial electronic transitions (green arrows). In the indirect process, SP decay produces excited carriers in the metal before the CT process (red arrows). In this mechanism, the spectra of the plasmonic nanostructure and the molecule do not need to overlap, but the energy of the excited carriers and the electronic band structure of the molecule need to match appropriately. Bearing the ultra-short lifetime of those SP-excited carriers in mind, the probability of such a photocatalysis-like process is usually low. Accordingly, for more efficient CT, the precursor should adsorb on the surface of the plasmonic structure. Combined with mediators such as semiconductors, the efficiency of plasmon-mediated chemical reactions (PMCRs) based on SP-excited carriers could greatly improve, as shown on the right. Such heterogeneous structures can increase the probability of CT and extend the lifetimes of the carriers transferred to the mediator, increasing the reaction probability. **c** | Increased temperature is commonly used to accelerate chemical reactions. The local temperature increase due to SP decay can increase the population of reactants in vibrationally excited states. SP decay also produces temperature increases that are highly localized at the surface where the chemical reaction occurs, which is a more efficient process than heating the whole reaction chamber. The thickness of the arrow represents the probability.

Factors influencing chemical reactions. Chemical reactions, especially catalytic processes, are closely related to surface activity. In PMCRs, three categories of mediators are usually used to improve the surface activity. To fully exploit the light harvesting effect, the plasmonic nanostructures (such as Au, Ag or Cu) should be larger than 5 nm, as opposed to standard catalysts for which larger sizes often limit their catalytic activity considerably[105]. Thus, in these cases, chemical reaction mediators, such as small-size Pt nanoparticles with high catalytic activity, are needed to construct composite structures to compensate for the loss of catalytic active sites. The lifetime of the plasmon-induced excited carriers is too short to participate effectively in the chemical reaction (FIG. 2b), leading to a low efficiency of charge transfer from the plasmonic nanostructure to the reaction precursor. Therefore, charge transfer mediators, such as semiconductors, are used to efficiently collect the excited carriers (FIGS 4b,5ba). For instance, by using ultrafast time-resolved spectroscopy, it has been shown that n-type TiO_2 can considerably promote efficient charge separation, thus inhibiting the recombination of non-equilibrated charge carriers[106]. However, to date, no consensus exists on what kind of mediator helps to achieve effective charge separation. SP-activated molecules (for example, O_2 and H_2) can also act as mediators. Some studies have found that O_2 activated by accepting an excited charge carrier from the plasmonic nanostructure can enhance catalytic oxidation reactions[86,87] (FIG. 5Bb).

Furthermore, processes including the adsorption and activation of the reactant, formation and retention of the intermediate, desorption of the resulting product and the mass transport of all the above species need also be taken into consideration in PMCRs, although few studies have fully explored these effects. It is preferential to carry out chemical reactions on structurally well-defined active sites where the reaction mechanism is straightforward and the SP effects for the chemical reaction can be easily understood.

Factors influencing the coupling between surface plasmons and adsorbed molecules. In order to efficiently coordinate SPs and reactants or mediators, attention should be paid to their coupling, which is strongly influenced by the surface or interface. Mediators, especially those for charge transfer, are coupled with the

plasmonic nanostructures to induce reactions and help increase the reaction rates[107–109]. In CdSe nanorods featuring a Au nanoparticle at each end, strong interdomain coupling and mixing of the metal and semiconductor energy levels lead to plasmon-induced interfacial charge transfer transition (PICTT). This enables the decay of a plasmon by directly exciting an electron from the metal to a strongly coupled acceptor[107] (FIG. 6a). In the case of metal–semiconductor contact, one can have two types of contacts: a Schottky contact and an Ohmic contact

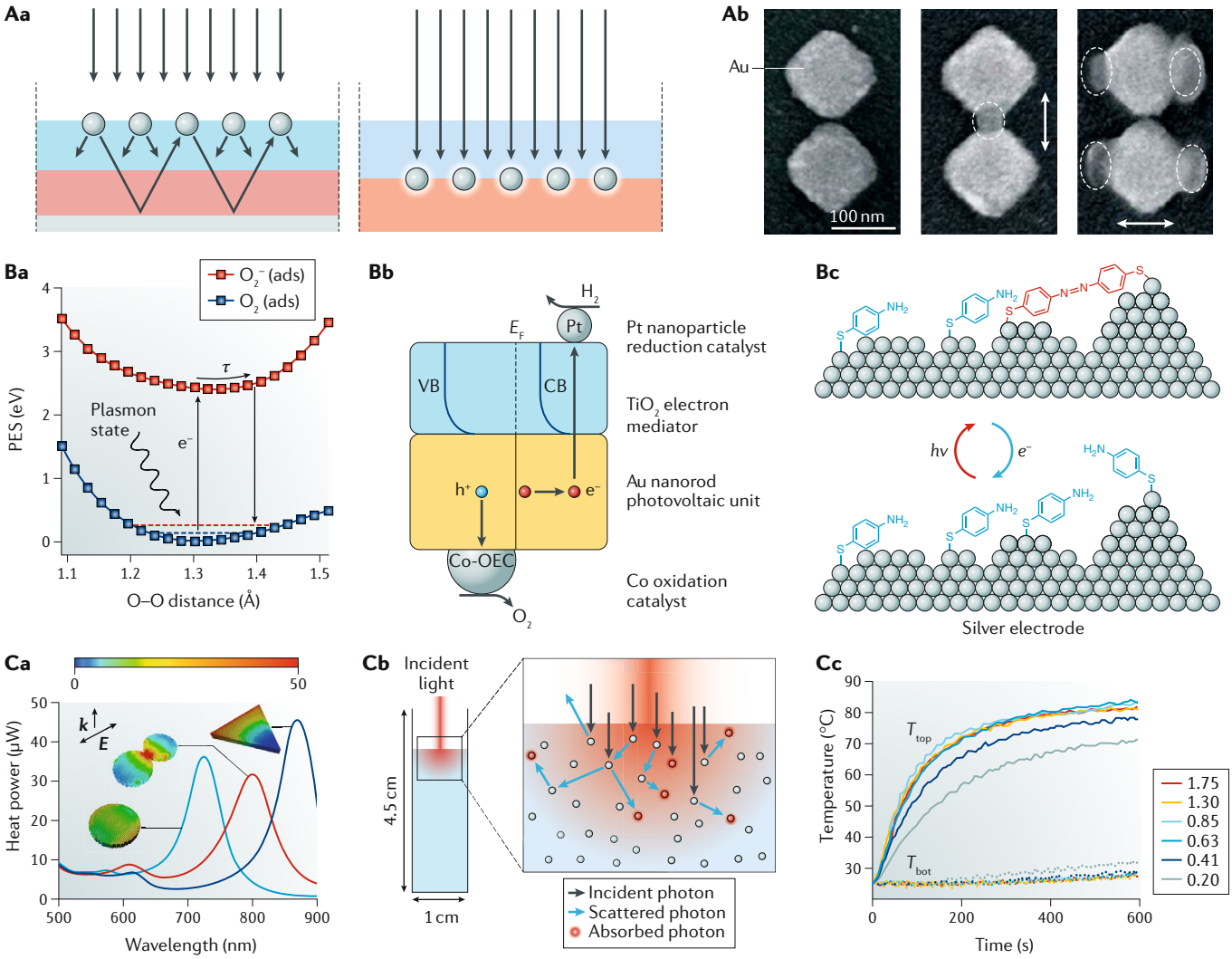

Fig. 5 | **The three key components of plasmon-mediated chemical reactions. A** | Electromagnetic near-field photochemical enhancement. **Aa** | Excitation probabilities induced by electromagnetic near-field enhancement increase with light intensity and light-path length. **Ab** | The electromagnetic near-field enhancement attained by controlling the direction of the polarized incident light can induce the two-photon polymerization of the photoresist SU8 along precise directions. **B** | Photocatalysis mediated by surface plasmon (SP)-excited carriers. **Ba** | The excited electrons transferred from Ag plasmonic nanostructures to an absorbed (ads) O_2 produce the transient negative-ion state of O_2^-, and its subsequent relaxation leads to vibrationally excited O_2 molecules. These activated oxygen molecules can act as the reaction mediator. τ depicts the transient negative-ion state of O_2^-. **Bb** | Schematic of a water splitting device in which the SP-induced excited carriers separate at the metal–mediator interface and participate in the redox process. Here, TiO_2 acts as the charge transfer mediator; Pt and Co-oxygen-evolving catalyst (OEC) nanoparticles act as mediators for the hydrogen evolution reaction and oxygen evolution reaction, respectively; CB, VB and E_F denote the conduction band, valence band and Fermi level, respectively. **Bc** | Scheme for the transformation from *p*-aminothiophenol (PATP) to *p,p′*-dimercaptoazobenzene (DMAB) induced by SP-excited electrons, which can be detected in situ by plasmon-enhanced Raman scattering. **C** | Local thermal effects promoted by SPs. **Ca** | Calculated spectra of the heat generated in nanostructures deposited on a planar glass surface immersed in water, where ***E*** is the electromagnetic field and ***k*** is the wave vector of incident light. The three insets represent the heat power density computed at the main plasmon resonance of the particle. The local heating is related to the morphology and incident light. The colour gradient indicates the heat power density (nW/nm³). **Cb** | Schematic of photoheating in a solution of nanoparticles illuminated with 808 nm laser light. Multiparticle optical interactions by which incident photons that are scattered and/or absorbed play an important role. **Cc** | Thermal response of illuminated nanoshell solutions with different concentrations (colour gradient shows the concentration denoted in units of 10^{10} per ml). The temperatures measured at the top (T_{top}) and bottom (T_{bot}) of the solutions are shown as solid and dashed lines. *hν*, energy of a photon; PES, potential energy surface; PMCRs, plasmon-mediated chemical reactions. Part **Aa** is adapted from REF.[75], Springer Nature Limited. Part **Ab** is adapted with permission from REF.[78], American Chemical Society. Part **Ba** is adapted from REF.[86], Springer Nature Limited. Part **Bb** is adapted from REF.[14], Springer Nature Limited. Part **Bc** is adapted with permission from REF.[26], American Chemical Society. Part **Ca** is adapted with permission from REF.[94], AIP Publishing. Parts **Cb** and **Cc** are adapted with permission from REF.[99], American Chemical Society.

(FIG. 6b). The nature of the contact between two materials forming a heterojunction (interface) can greatly influence the charge transfer process of the excited carriers. For example, the energy barrier formed upon Schottky contact can be used to filter the excited electrons, inhibiting their recombination with holes. Ohmic contact, on the other hand, can permit the transfer of low-energy excited electrons, such as electrons induced by interband transitions, through the interface, from the plasmonic metal to the semiconductor[108]. Alternatively, a SiO_2 layer with a thickness of about 5 nm can be used to isolate the plasmonic nanostructure from the semiconductor (for example, Cu_2O), so that the plasmon-induced resonance energy transfer (PIRET), which is strongly dependent on the dephasing rate and dipole moment of the plasmon, can be tuned[109] (FIG. 6c).

Surfactants are also used to stabilize the surface of the plasmonic nanostructure and to avoid aggregation and can affect the plasmonic properties and surface reactions. Additionally, SP effects, such as the enhanced electromagnetic near-field, are strongly dependent on the distance of the SPs from the surface. Close proximity to the surface is usually more beneficial for PMCRs.

Comparison of PEMS and PMCRs

As two important branches of plasmonics, PEMS and PMCRs are closely related, and both result from three-body interactions between photons, molecules and nanostructures (FIG. 7a,b). However, the study of PMCRs (plasmon chemistry) is more complex than PEMS (plasmon physics) because it involves molecular changes, for which many factors, such as reaction intermediates, products and yields as well as charge transfer rates, must be taken into account (TABLE 1). This is likely the reason why the development of PMCRs has lagged behind that of PEMS. It is therefore desirable to systematically analyse the similarities and major differences between these two branches of plasmonics in order to identify challenges and future directions in plasmonic chemistry.

PERS is the most established technique among PEMS and has been applied for over four decades[5–8,11]. Here, we use PERS as a representative to compare and contrast PEMS and PMCR.

The electromagnetic near-field enhancement

In PERS, electromagnetic enhancement promotes both excitation and emission. Emission, however, is absent in the case of PMCRs based on electromagnetic near-field owing to the non-radiative decay of excited states via chemical reactions. Moreover, the excitation of the reacting molecules or mediators in PMCRs includes an electron transition from the electronic ground state to the real excited state[76,77]. In PERS, the electrons in the ground state are usually excited to a virtual state, except in cases of resonance or stimulated Raman scattering[11,56].

The surface-plasmon-excited charge carriers

Charge transfer between the plasmonic nanostructure and the reactant molecule plays a key role in PMCRs[16,107]. Such processes can also be important in PERS when the plasmonic nanostructure forms a strong bond with the probed molecule[67]. The main difference between charge transfer in PMCRs and in PERS is the final destination of the excited carriers. In PMCRs, carriers are excited and separated in order to participate in the chemical reaction, which takes place at the interface between the metal and the surrounding medium (FIG. 4b). It should be noted that to increase the probability of participating in chemical reactions, the excited

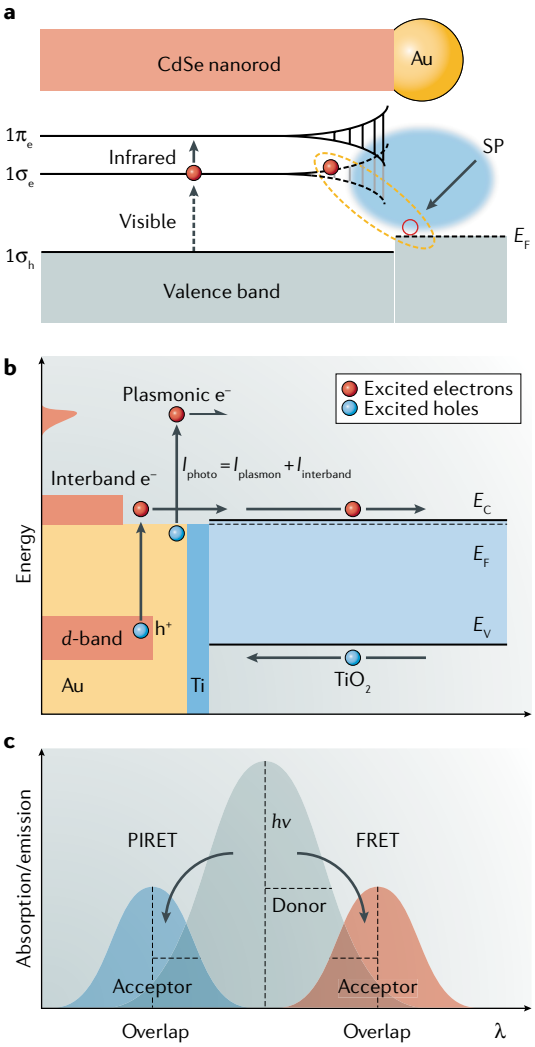

Fig. 6 | **A graphical summary of novel mechanisms of SP-mediated energy and/or charge transfer processes.** **a** | The plasmon-induced interfacial charge transfer taking place at a metal–semiconductor interface (Au–CdSe) with strong coupling. **b** | Ohmic devices (in this case, Au–Ti–TiO_2) enable surface plasmon (SP)-excited electrons with high energy ($I_{plasmon}$) and excited electrons created by interband transitions ($I_{interband}$) to be collected, thus enhancing the photocurrent I_{photo}. **c** | Plasmon-induced resonance energy transfer (PIRET). PIRET is different from Förster resonance energy transfer (FRET) because of the lack of a Stokes shift and a strong dependence on the dephasing rate and dipole moment of the plasmon. E_C, conduction-band energy; E_F, Fermi level; E_V, valence-band energy; $h\nu$, energy of a photon; λ, wavelength. Part **a** is adapted with permission from REF.[107], AAAS. Part **b** is adapted from REF.[108], Springer Nature Limited. Part **c** is adapted from REF.[109], Springer Nature Limited.

Förster resonance energy transfer
(FRET). A mechanism describing the energy transfer between two light-sensitive dipoles, in which energy non-radiatively transfers from a blueshifted emitter to a redshifted absorber through dipole–dipole coupling.

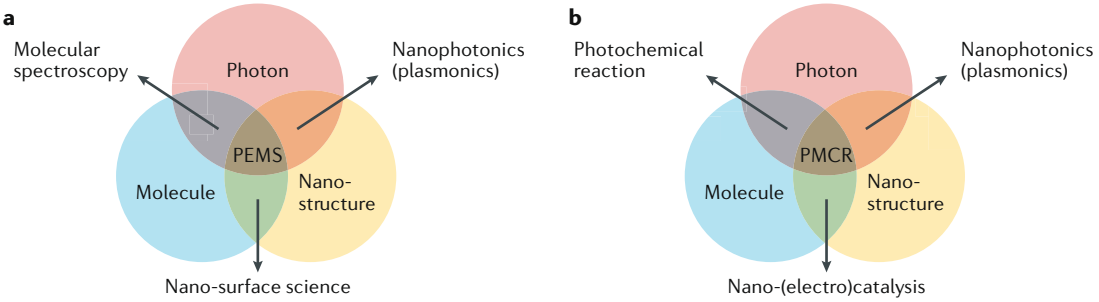

Fig. 7 | **Comparison of plasmon-enhanced molecular spectroscopy and plasmon-mediated chemical reactions.** **a** | The three-body interaction in plasmon-enhanced molecular spectroscopy (PEMS), which includes a photon, nanostructure and molecule (that does not undergo chemical reactions). When only two of the three elements interact, three separate fields arise: nanophotonics, nano-surface science and molecular spectroscopy. **b** | The three-body interactions in plasmon-mediated chemical reactions (PMCRs), which also includes a photon, nanostructure and molecule (that undergoes chemical reactions). The interaction of only two of the three elements gives rise to different kinds of reactions and processes.

carriers in PMCRs should occupy the orbitals of reactants for a long time. Nevertheless, the excited carriers in the charge transfer process of PERS quickly decay back to the metal or the surface complex on a femtosecond timescale (FIG. 3b).

The heating effect

Local heating is common but often ignored in plasmonic systems. There have been only a few systematic studies on the local heating effect in PMCRs[96]. Increased temperature can lead to increased reaction rate by providing energy to overcome the energy barrier of the reaction and by promoting mass transport and surface desorption. In contrast, increased temperature can hamper PERS measurements that are easier for strongly adsorbed molecules. Additionally, the local heating of SPs leads to a confined thermal field with steep gradients. The reactions that proceed in the confined high-temperature region can, in turn, influence the distribution of the thermal field. For example, if the reaction is exothermic, the heat of reaction may further increase the temperature gradients.

Determining the local temperature in the presence of gradients is challenging but essential for understanding reaction mechanisms and designing PMCRs. Local heating may also affect PEMS measurements. For example, it was observed in some PERS measurements that the Stokes and anti-Stokes Raman scattering processes are asymmetrically enhanced with a preferential increase in the anti-Stokes Raman bands[110]. This was first proposed to be due to the laser-induced thermal heating ('pumping') of the ground-state molecule that promotes the population of the vibrationally excited states[111]. Accordingly, the Boltzmann equation was used to calculate the local temperature rise due to the non-radiative, thermal decay of the plasmon based on the PERS characteristics[112,113]. Many disagreements remain surrounding such calculation and the other factors involved in the enhancement of the anti-Stokes Raman bands in PERS[114–116]. For example, it has been found that other effects, such as a broad and intense plasmon resonance, can affect the ratio of the anti-Stokes and Stokes intensity[117,118]. Thus, in order to use this intensity ratio to calculate the local temperature, one should first normalize the PERS spectra against the plasmon resonance spectra (which reflects the SP enhancement difference in different frequency regions) over the whole frequency region[117]. Furthermore, PERS measurements are usually averaged over multiple hot spots, medium-enhanced regions and non-enhanced regions. The geometric inhomogeneity of these regions represents an additional problem when PERS is used to determine the local temperature. The system becomes even more complex when chemical enhancement and/or charge transfer need to be taken into consideration.

Future challenges and directions

Despite the fact that PMCR mechanisms can be explained by thermochemistry, photochemistry and/or photocatalysis, PMCRs are more complex than traditional reactions. The probable combination of all three mechanisms, especially in a nano-confined space, leads to some of the unique characteristics of PMCRs. The local confinement of the electromagnetic field and thermal field causes the heterogeneous distribution of the reactive area on a substrate. In order to fully take advantage of PMCRs, one needs to carefully analyse the challenges and future directions according to the following five aspects.

New plasmonic structures and materials

The structure and composition of the plasmonic nanostructures are two crucial factors that control the spatial (position), energetic (strength and wavelength) and temporal (lifetime) properties of SPs[48]. Nanostructures with tuneable plasmonic properties would be useful in PMCRs, as it would be possible to design tuneable SPs with either a narrowband or broadband response, to control the energy distribution and lifetime of the excited carriers and to increase the charge transfer probability. For example, a narrowband response can be used to finely regulate the energy of the incident light, which can then be used to control the energy flow that mediates the reaction or to regulate the reaction selectivity of certain molecules. The broadband response, instead, is mainly exploited to increase the efficiency of solar energy utilization, especially for reactions with various reactants but without selectivity requirements, such as pollutant degradation.

Table 1 | **Comparison of PEMS and PMCRs**

Effect	PEMS (PERS 1970s–today)	PMCRs (1980s–today)
EM field enhancement	Primary effect; it enhances the probability of electronic excitation to virtual and/or real states	Favourable effect; it enhances the probability of electronic excitations to real states
Excited carriers	Secondary effect; excited carriers are transferred back and forth from the nanoplasmonic structure to the adsorbed molecule	Favourable effect; excited carriers are transferred from the nanoplasmonic structure to the adsorbed molecule to mediate a reaction
Heating	Unfavourable effect; causes desorption or damage to the adsorbed molecule	Favourable effect; helps to overcome the activation energy barrier
Local effects	Creates hot spots, which contribute most of the spectral signal (<10 nm)	Confines the chemical reaction to proceeding over small spatial scales (nm–μm)
Components		
Light source	A focused laser is most commonly used (<0.1 bandwidth, 10^6–10^8 mW/cm^2)	Solar simulator, Xe lamp, Hg lamp, LED or lasers, among others (10^2–10^8 mW/cm^2)
Molecule	Strong adsorption of the probed molecule on the plasmonic surface is favourable	Strong adsorption of reactants, mediators and products may impede reactions
Nanostructures	Simple structures made of plasmonic-active materials	Complex structures made of plasmonic materials coupled with mediators for surface activation and charge transfer

EM, electromagnetic; LED, light-emitting diode; PEMS, plasmon-enhanced molecular spectroscopy; PERS, plasmon-enhanced Raman spectroscopy; PMCRs, plasmon-mediated chemical reactions.

Notably, a compromise between the catalytic activity and the strong optical effect is widely observed in PMCRs when coinage metals are used. Methods that use, for example, antenna-reactors, satellite or core–shell composite structures have been adopted[16,119–121]. Most of these consist of two typical components: a highly active plasmonic nanostructure and a highly active catalyst. In addition, expanding the range of plasmonic materials to better accommodate PMCRs is highly desirable. Some novel materials, such as graphene, have also been shown to have SP properties[122]. It is important to choose suitable materials for specific applications or chemical reactions[123–125]. Some of these plasmonic materials are usually used as catalysts. However, for these materials, the plasmon resonance frequencies usually are not in the visible or near-infrared region. Developing plasmonic materials responsive to sunlight with high catalytic activity represents an important goal in the field of PMCRs.

Multiscale processes

Electromagnetic near-field, charge-carrier excitation and local heating effects are usually concurrent in PMCRs, but it would be useful to determine which is crucial for a specific reaction. However, the systematic study of these effects is hindered by the extended timescales (spanning from several femtoseconds to nanoseconds) and highly confined space over which the reactions evolve[29,36–38]. Several strategies have been exploited to solve this problem, such as using insulating materials like silica to prevent charge transfer. However, the silica coating also changes the surface and thermal properties of the plasmonic nanostructure and influences the resonant energy transfer from the plasmonic nanostructure to the mediator or molecule[109,126]. Therefore, new methods that are less invasive to the sample and the reaction need to be developed.

Plasmon-induced excited carriers

Although plasmon-induced excited carriers have proved effective in many important reactions[14,86,90,91], the efficiencies of plasmon-mediated photocatalysis remain low, and mediators must be used. For example, a well-designed system containing a charge separation mediator and a reaction mediator has been used to catalyse water splitting upon irradiation with visible light, leading to the highest reported external quantum efficiency of approximately 0.1%[14]. Obviously, excited carriers in metals are different from those in semiconductors owing to the lack of bandgap[82,83], which gives rise to extremely short lifetimes of the plasmon-induced excited carriers and hinders charge transfer even in the presence of mediators[33,35–40]. In some special cases, such as strong coupling, the charge transfer efficiency may be enhanced considerably (although no breakthrough has yet been reported for the overall reaction efficiency), and some new charge transfer mechanisms, such as SP-induced interfacial charge transfer, have been proposed[107] (FIGS 4b,6a). However, some key questions remain even with respect to the charge transfer mechanism, for example, about the strong coupling between SPs and molecules[127,128]. The energy distribution of plasmon-induced excited carriers is different from that in a semiconductor and the interband transition process of the plasmonic material. More precisely, in the former case, the *sp*-bands are supposed to be diffuse and have relatively constant density of states in the range of visible energy (using the Fermi level as a reference), which probably lead to a flat distribution of excited carriers[18,40], although little experimental evidence for this can be cited. Finally, the properties of excited holes are still poorly understood, with only a few direct experiments describing their characteristics, such as their energy distribution and lifetimes[129].

The confinement effect

Many materials, including semiconductors and dyes, can provide excited carriers but are unable to confine the corresponding electric and thermal fields at the nanoscale. SP effects can not only result in a spatial redistribution of the optical, electronic and/or thermal energy at the nanoscale but can also endow the local field with steep gradients[1,2,17,75]. In PMCRs, the spatial distribution of the electromagnetic field, thermal field and excited carriers is non-uniform[130]. Therefore, the localized effect of SPs should directly lead to a localized chemical reaction[131], as was demonstrated in metal–polymer–metal systems[132]. Scanning tunnelling microscopy (STM) with a Ag tip was used to achieve the real-space and real-time observation of a PMCR, which indicated the spatial inhomogeneity of the PMCR[133]. Additionally, the localized effect can influence many physical processes related to chemical reactions, including heat transfer and mass transport[98]. More advanced applications, especially scalable ones, based on the localized effect will require more than a few hot spots and large active surfaces. Expanding the ratio of highly active sites is crucial for PMCRs but also would ensure higher sensitivity in PERS.

Bond-selective reactions

Tip-enhanced Raman spectroscopy can access the structure and conformation of a single molecule with both chemical accuracy and sub-nanometre resolution[59,134]. The ultra-high spatial resolution is thought to result from the highly confined field and broadband nature of the nanocavity plasmons in the tunnelling gap between the tip and substrate[135]. This crucial breakthrough offers a new way to simultaneously gain structural and chemical information of single molecules by means of PERS. More interestingly, the ultra-high spatial resolution enables the manipulation of specific parts of a single molecule (for example, a methyl group or a double bond) within a single molecule under plasmonic excitation. This may result in a new, submicroscopic level of molecular processing.

Heavily doped semiconductors have been shown to have excellent plasmonic properties in the mid-infrared or far-infrared region[136,137], and selective infrared femtosecond laser pulse excitation has been reported to accelerate ground-state reactions[138]. Accordingly, SPs in the mid-infrared region could also be used to excite the vibrational modes of molecules for PMCRs or PEMS. More importantly, it may provide a new opportunity to excite chemical bonds for bond-selective chemistry, if the band response of SPs is narrow enough.

Conclusion

We have reviewed the progress in using nanostructure-based SPs as mediators to redistribute and convert the photon energy in time, in space and at various energy scales, thereby driving chemical reactions by localizing photon, electronic and/or thermal energies. PMCRs exhibit unique characteristics distinct from existing photoenhanced and thermally enhanced reactions. For instance, the electromagnetic field and/or thermal field in PMCRs are confined at the nanoscale with sharp gradients (sub-nanometre to nanometre for electromagnetic fields and nanometre to micrometre for thermal fields), which can drive chemical reactions at an extreme level of spatial selectivity. In such cases, both the nano-optics and nano-thermodynamics are unique and offer opportunities through, for example, the nano-confinement of mass or facile heat transfer, for novel reaction pathways with increased efficiencies or product branching possibilities. Additionally, the lifetime (less than picoseconds) and the flat energy distribution of the excited carriers in PMCRs differ from what is encountered in traditional photocatalysis (the excited carriers distribute in definite bands with picosecond to microsecond lifetimes). As a consequence, SPs can create new possibilities for powering chemical reactions.

The field of PMCRs is still in an early stage, and two main challenges hinder its rapid development: the complex operating mechanism and the limited reaction efficiencies, especially when based on the excited carriers. PEMS has been developed over 40 years and can serve as a reference for guiding the progress of PMCRs. PEMS and PMCRs are both molecule-specific and dependent on three-body (molecule, incident photon and plasmonic nanostructure) interactions. To clearly describe the mechanism of PMCRs, we systematically introduced various effects over time, space and energy scales. However, to improve the efficiency, one needs to coordinate these effects synergistically. Great advancements will be made, for example, by rationally designing and fabricating plasmonic nanostructures, selecting suitable surface or interface mediators and teaming them together.

Published online 30 August 2018

1. Schuller, J. A. et al. Plasmonics for extreme light concentration and manipulation. *Nat. Mater.* **9**, 193–204 (2010).
2. Barnes, W. L., Dereux, A. & Ebbesen, T. W. Surface plasmon subwavelength optics. *Nature* **424**, 824–830 (2003).
3. Fleischmann, M., Hendra, P. J. & McQuillan, A. J. Raman spectra of pyridine adsorbed at a silver electrode. *Chem. Phys. Lett.* **26**, 163–166 (1974).
4. Jeanmaire, D. L. & Van Duyne, R. P. Surface Raman spectroelectrochemistry: Part I. Heterocyclic, aromatic, and aliphatic amines adsorbed on the anodized silver electrode. *J. Electroanal. Chem. Interfacial Electrochem.* **84**, 1–20 (1977).
5. Moskovits, M. Surface roughness and the enhanced intensity of Raman scattering by molecules adsorbed on metals. *J. Chem. Phys.* **69**, 4159–4161 (1978).
6. Moskovits, M. Surface-enhanced spectroscopy. *Rev. Mod. Phys.* **57**, 783–826 (1985).
7. Tian, Z. Q., Ren, B. & Wu, D. Y. Surface-enhanced Raman scattering: from noble to transition metals and from rough surfaces to ordered nanostructures. *J. Phys. Chem. B* **106**, 9463–9483 (2002).
8. Ding, S. Y., You, E. M., Tian, Z. Q. & Moskovits, M. Electromagnetic theories of surface-enhanced Raman spectroscopy. *Chem. Soc. Rev.* **46**, 4042–4076 (2017).
9. Lal, S., Clare, S. E. & Halas, N. J. Nanoshell-enabled photothermal cancer therapy: Impending clinical impact. *Acc. Chem. Res.* **41**, 1842–1851 (2008).
10. Mayer, K. M. & Hafner, J. H. Localized surface plasmon resonance sensors. *Chem. Rev.* **111**, 3828–3857 (2011).
11. Stiles, P. L., Dieringer, J. A., Shah, N. C. & Van Duyne, R. P. Surface-enhanced Raman spectroscopy. *Annu. Rev. Anal. Chem.* **1**, 601–626 (2008).
12. Emmanuel, F. & Samuel, G. Surface enhanced fluorescence. *J. Phys. D Appl. Phys.* **41**, 013001 (2008).
13. Zhou, L. et al. 3D self-assembly of aluminium nanoparticles for plasmon-enhanced solar desalination. *Nat. Photon.* **10**, 393 (2016).
14. Mubeen, S. et al. An autonomous photosynthetic device in which all charge carriers derive from surface plasmons. *Nat. Nanotech.* **8**, 247–251 (2013).
15. Linic, S., Christopher, P. & Ingram, D. B. Plasmonic-metal nanostructures for efficient conversion of solar to chemical energy. *Nat. Mater.* **10**, 911–921 (2011).
16. Clavero, C. Plasmon-induced hot-electron generation at nanoparticle/metal-oxide interfaces for photovoltaic and photocatalytic devices. *Nat. Photon.* **8**, 95–103 (2014).

17. Baffou, G. & Quidant, R. Nanoplasmonics for chemistry. *Chem. Soc. Rev.* **43**, 3898–3907 (2014).
18. Christopher, P. & Moskovits, M. Hot charge carrier transmission from plasmonic nanostructures. *Annu. Rev. Phys. Chem.* **68**, 379–398 (2017).
19. Ostovar pour, S. et al. Through-space transfer of chiral information mediated by a plasmonic nanomaterial. *Nat. Chem.* **7**, 591 (2015).
20. Nitzan, A. & Brus, L. E. Theoretical model for enhanced photochemistry on rough surfaces. *J. Chem. Phys.* **75**, 2205–2214 (1981).
21. Chen, C. J. & Osgood, R. M. Direct observation of the local-field-enhanced surface photochemical reactions. *Phys. Rev. Lett.* **50**, 1705–1708 (1983).
22. Chen, X. J., Cabello, G., Wu, D. Y. & Tian, Z. Q. Surface-enhanced Raman spectroscopy toward application in plasmonic photocatalysis on metal nanostructures. *J. Photochem. Photobiol. C* **21**, 54–80 (2014).
23. Suh, J. S., Moskovits, M. & Shakhesemampour, J. Photochemical decomposition at colloid surfaces. *J. Phys. Chem.* **97**, 1678–1683 (1993).
24. Suh, J. S., Jang, N. H., Jeong, D. H. & Moskovits, M. Adsorbate photochemistry on a colloid surface: phthalazine on silver. *J. Phys. Chem.* **100**, 805–813 (1996).
25. Brus, L. Noble metal nanocrystals: Plasmon electron transfer photochemistry and single-molecule Raman spectroscopy. *Acc. Chem. Res.* **41**, 1742–1749 (2008).
26. Huang, Y. F. et al. When the signal is not from the original molecule to be detected: chemical transformation of para-Aminothiophenol on Ag during the SERS measurement. *J. Am. Chem. Soc.* **132**, 9244–9246 (2010).
27. Wimmer, E., Fu, C. L. & Freeman, A. J. Catalytic promotion and poisoning: all-electron Local-density-functional theory of CO on Ni(001) surfaces coadsorbed with K or S. *Phys. Rev. Lett.* **55**, 2618–2621 (1985).
28. Alayoglu, S., Nilekar, A. U., Mavrikakis, M. & Eichhorn, B. Ru-Pt core-shell nanoparticles for preferential oxidation of carbon monoxide in hydrogen. *Nat. Mater.* **7**, 333–338 (2008).
29. Ozbay, E. Plasmonics: merging photonics and electronics at nanoscale dimensions. *Science* **311**, 189–193 (2006).
30. Maier, S. A. et al. Local detection of electromagnetic energy transport below the diffraction limit in metal nanoparticle plasmon waveguides. *Nat. Mater.* **2**, 229–232 (2003).
31. Le Ru, E. C. & Etchegoin, P. G. in *Principles of Surface-Enhanced Raman Spectroscopy* Ch. 3, 121–183 (Elsevier, Amsterdam, 2009).
32. Maier, S. A. in *Plasmonics: fundamentals and applications* Ch. 5 (Springer Science & Business Media, 2007).
33. Link, S. & El-Sayed, M. A. Spectral properties and relaxation dynamics of surface plasmon electronic oscillations in gold and silver nanodots and nanorods. *J. Phys. Chem. B* **103**, 8410–8426 (1999).
34. Hao, F. et al. Symmetry breaking in plasmonic nanocavities: subradiant LSPR sensing and a tunable Fano resonance. *Nano Lett.* **8**, 3983–3988 (2008).
35. Frischkorn, C. & Wolf, M. Femtochemistry at metal surfaces: nonadiabatic reaction dynamics. *Chem. Rev.* **106**, 4207–4233 (2006).
36. Khurgin, J. B. How to deal with the loss in plasmonics and metamaterials. *Nat. Nanotech.* **10**, 2–6 (2015).
37. Cho, G. C., Dekorsy, T., Bakker, H. J., Hövel, R. & Kurz, H. Generation and relaxation of coherent majority plasmons. *Phys. Rev. Lett.* **77**, 4062–4065 (1996).
38. Inouye, H., Tanaka, K., Tanahashi, I. & Hirao, K. Ultrafast dynamics of nonequilibrium electrons in a gold nanoparticle system. *Phys. Rev. B* **57**, 11334–11340 (1998).
39. Bonn, M. et al. Phonon- versus electron-mediated desorption and oxidation of CO on Ru(0001). *Science* **285**, 1042–1045 (1999).
40. Brongersma, M. L., Halas, N. J. & Nordlander, P. Plasmon-induced hot carrier science and technology. *Nat. Nanotech.* **10**, 25–34 (2015).
41. Osawa, M., Ataka, K. I., Yoshii, K. & Nishikawa, Y. Surface-enhanced infrared spectroscopy: the origin of the absorption enhancement and band selection rule in the infrared spectra of molecules adsorbed on fine metal particles. *Appl. Spectrosc.* **47**, 1497–1502 (1993).
42. Aroca, R. F., Ross, D. J. & Domingo, C. Surface-enhanced infrared spectroscopy. *Appl. Spectrosc.* **58**, 324A–338A (2004).
43. Ortolani, M. & Limaj, O. in *Handbook of Enhanced Spectroscopy* 443–483 (Pan Stanford, 2015).
44. Tian, Z. Q., Ren, B., Li, J. F. & Yang, Z. L. Expanding generality of surface-enhanced Raman spectroscopy with borrowing SERS activity strategy. *Chem. Commun.* **34**, 3514–3534 (2007).
45. Stadler, J., Schmid, T. & Zenobi, R. Developments in and practical guidelines for tip-enhanced Raman spectroscopy. *Nanoscale* **4**, 1856–1870 (2012).
46. Li, J. F., Anema, J. R., Wandlowski, T. & Tian, Z. Q. Dielectric shell isolated and graphene shell isolated nanoparticle enhanced Raman spectroscopies and their applications. *Chem. Soc. Rev.* **44**, 8399–8409 (2015).
47. Gruenke, N. L. et al. Ultrafast and nonlinear surface-enhanced Raman spectroscopy. *Chem. Soc. Rev.* **45**, 2263–2290 (2016).
48. Ding, S. Y. et al. Nanostructure-based plasmon-enhanced Raman spectroscopy for surface analysis of materials. *Nat. Rev. Mater.* **1**, 16021 (2016).
49. Li, J. F., Li, C. Y. & Aroca, R. F. Plasmon-enhanced fluorescence spectroscopy. *Chem. Soc. Rev.* **46**, 3962–3979 (2017).
50. Gray, S. K. Surface plasmon-enhanced spectroscopy and photochemistry. *Plasmonics* **2**, 143–146 (2007).
51. Le Ru, E. C. & Etchegoin, P. G. in *Principles of Surface-Enhanced Raman Spectroscopy*. 185–264 (Elsevier Science, 2008).
52. Etchegoin, P. G. & Le Ru, E. C. in *Surface Enhanced Raman Spectroscopy* (ed. Schlucker, S.) 1–37 (Wiley VCH, 2010).
53. Ding, S. Y., Zhang, X. M., Ren, B. & Tian, Z. Q. in *Encyclopedia of Analytical Chemistry* (Wiley-Blackwell, 2006).
54. Wang, X. et al. Tip-enhanced Raman spectroscopy for surfaces and interfaces. *Chem. Soc. Rev.* **46**, 4020–4041 (2017).
55. Schmid, T., Opilik, L., Blum, C. & Zenobi, R. Nanoscale chemical imaging using tip-enhanced Raman spectroscopy: a critical review. *Angew. Chem. Int. Ed.* **52**, 5940–5954 (2013).
56. Schlücker, S. Surface-enhanced Raman spectroscopy: Concepts and chemical applications. *Angew. Chem. Int. Ed.* **53**, 4756–4795 (2014).
57. Michaels, A. M., Nirmal, M. & Brus, L. E. Surface enhanced Raman spectroscopy of individual Rhodamine 6G molecules on large Ag nanocrystals. *J. Am. Chem. Soc.* **121**, 9932–9939 (1999).
58. Nie, S. & Emory, S. R. Probing single molecules and single nanoparticles by surface-enhanced Raman scattering. *Science* **275**, 1102–1106 (1997).
59. Zhang, R. et al. Chemical mapping of a single molecule by plasmon-enhanced Raman scattering. *Nature* **498**, 82–86 (2013).
60. Yampolsky, S. et al. Seeing a single molecule vibrate through time-resolved coherent anti-Stokes Raman scattering. *Nat. Photon.* **8**, 650–656 (2014).
61. Kerker, M., Wang, D. S. & Chew, H. Surface enhanced Raman scattering (SERS) by molecules adsorbed at spherical particles. *Appl. Opt.* **19**, 3373–3388 (1980).
62. Gersten, J. & Nitzan, A. Electromagnetic theory of enhanced Raman scattering by molecules adsorbed on rough surfaces. *J. Chem. Phys.* **73**, 3023–3037 (1980).
63. Aravind, P. K., Nitzan, A. & Metiu, H. The interaction between electromagnetic resonances and its role in spectroscopic studies of molecules adsorbed on colloidal particles or metal spheres. *Surf. Sci.* **110**, 189–204 (1981).
64. Le Ru, E. & Etchegoin, P. in *Principles of Surface-Enhanced Raman Spectroscopy* Ch. 2 (Elsevier, Amsterdam, 2009).
65. Otto, A. *Surface-enhanced Raman scattering: "Classical" and "Chemical" origins* (Springer Berlin Heidelberg, 1984).
66. Tian, Z. Q. General Discussion. *Faraday Discuss.* **132**, 147–158 (2006).
67. Wu, D. Y., Li, J. F., Ren, B. & Tian, Z. Q. Electrochemical surface-enhanced Raman spectroscopy of nanostructures. *Chem. Soc. Rev.* **37**, 1025–1041 (2008).
68. Schatz, G. C. & Van Duyne, R. P. in *Handbook of Vibrational Spectroscopy* (John Wiley & Sons, Ltd, 2006).
69. Klessinger, M. & Michl, J. *Excited States and Photochemistry of Organic Molecules* (VCH Publishers, New York, 1995).
70. Turro, N. J. *Modern Molecular Photochemistry* (Univ. Science Books, Mill Valley, CA, 1991).
71. Karny, Z. & Zare, R. N. Infrared laser photochemistry: Evidence for heterogeneous decomposition. *Chem. Phys.* **23**, 321–325 (1977).
72. Zare, R. N. Laser control of chemical reactions. *Science* **279**, 1875–1879 (1998).
73. Ottosson, H. Exciting excited-state aromaticity. *Nat. Chem.* **4**, 969 (2012).
74. Van Leeuwen, T., Lubbe, A. S., Štacko, P., Wezenberg, S. J. & Feringa, B. L. Dynamic control of function by light-driven molecular motors. *Nat. Rev. Chem.* **1**, 0096 (2017).
75. Atwater, H. A. & Polman, A. Plasmonics for improved photovoltaic devices. *Nat. Mater.* **9**, 205–213 (2010).
76. Liu, Z., Hou, W., Pavaskar, P., Aykol, M. & Cronin, S. B. Plasmon resonant enhancement of photocatalytic water splitting under visible illumination. *Nano Lett.* **11**, 1111–1116 (2011).
77. Ingram, D. B. & Linic, S. Water splitting on composite plasmonic-metal/semiconductor photoelectrodes: Evidence for selective plasmon-induced formation of charge carriers near the semiconductor surface. *J. Am. Chem. Soc.* **133**, 5202–5205 (2011).
78. Ueno, K. et al. Nanoparticle plasmon-assisted two-photon polymerization induced by incoherent excitation source. *J. Am. Chem. Soc.* **130**, 6928–6929 (2008).
79. Murdoch, M. et al. The effect of gold loading and particle size on photocatalytic hydrogen production from ethanol over Au/TiO_2 nanoparticles. *Nat. Chem.* **3**, 489 (2011).
80. Roger, I., Shipman, M. A. & Symes, M. D. Earth-abundant catalysts for electrochemical and photoelectrochemical water splitting. *Nat. Rev. Chem.* **1**, 0003 (2017).
81. Honda, K. & Fujishima, A. Electrochemical photolysis of water at a semiconductor electrode. *Nature* **238**, 37–38 (1972).
82. Linsebigler, A. L., Lu, G. & Yates, J. T. Photocatalysis on TiO_2 surfaces: principles, mechanisms, and selected results. *Chem. Rev.* **95**, 735–758 (1995).
83. Wang, Q. et al. Scalable water splitting on particulate photocatalyst sheets with a solar-to-hydrogen energy conversion efficiency exceeding 1%. *Nat. Mater.* **15**, 611–615 (2016).
84. Denzler, D. N., Frischkorn, C., Hess, C., Wolf, M. & Ertl, G. Electronic excitation and dynamic promotion of a surface reaction. *Phys. Rev. Lett.* **91**, 226102 (2003).
85. Tian, Y. & Tatsuma, T. Plasmon-induced photoelectrochemistry at metal nanoparticles supported on nanoporous TiO_2. *Chem. Commun.* 1810–1811 (2004).
86. Christopher, P., Xin, H. & Linic, S. Visible-light-enhanced catalytic oxidation reactions on plasmonic silver nanostructures. *Nat. Chem.* **3**, 467–472 (2011).
87. Huang, Y. F. et al. Activation of oxygen on gold and silver nanoparticles assisted by surface plasmon resonances. *Angew. Chem. Int. Ed.* **53**, 2353–2357 (2014).
88. Xie, W. & Schlücker, S. Hot electron-induced reduction of small molecules on photorecycling metal surfaces. *Nat. Commun.* **6**, 7570 (2015).
89. Mukherjee, S. et al. Hot-electron-induced dissociation of H_2 on gold nanoparticles supported on SiO_2. *J. Am. Chem. Soc.* **136**, 64–67 (2014).
90. Martirez, J. M. P. & Carter, E. A. Excited-state N_2 dissociation pathway on Fe-functionalized Au. *J. Am. Chem. Soc.* **139**, 4390–4398 (2017).
91. Hou, W. et al. Photocatalytic conversion of CO_2 to hydrocarbon fuels via plasmon-enhanced absorption and metallic interband transitions. *ACS Catal.* **1**, 929–936 (2011).
92. Oshikiri, T., Ueno, K. & Misawa, H. Plasmon-induced ammonia synthesis through nitrogen photofixation with visible light irradiation. *Angew. Chem. Int. Ed.* **53**, 9802–9805 (2014).
93. Zhang, N. et al. Near-field dielectric scattering promotes optical absorption by platinum nanoparticles. *Nat. Photon.* **10**, 473–482 (2016).
94. Baffou, G., Quidant, R. & Girard, C. Heat generation in plasmonic nanostructures: Influence of morphology. *Appl. Phys. Lett.* **94**, 153109 (2009).
95. Baffou, G. & Quidant, R. Thermo-plasmonics: using metallic nanostructures as nano-sources of heat. *Laser Photon. Rev.* **7**, 171–187 (2013).
96. Cao, L., Barsic, D. N., Guichard, A. R. & Brongersma, M. L. Plasmon-assisted local temperature control to pattern individual semiconductor nanowires and carbon nanotubes. *Nano Lett.* **7**, 3523–3527 (2007).

97. Yang, Q., Xu, Q., Yu, S. H. & Jiang, H. L. Pd Nanocubes@ZIF-8: integration of plasmon-driven photothermal conversion with a metal-organic framework for efficient and selective catalysis. *Angew. Chem. Int. Ed.* **55**, 3685–3689 (2016).
98. Kim, K. et al. Radiative heat transfer in the extreme near field. *Nature* **528**, 387–391 (2015).
99. Hogan, N. J. et al. Nanoparticles heat through light localization. *Nano Lett.* **14**, 4640–4645 (2014).
100. Govorov, A. O., Zhang, H., Demir, H. V. & Gun'ko, Y. K. Photogeneration of hot plasmonic electrons with metal nanocrystals: quantum description and potential applications. *Nano Today* **9**, 85–101 (2014).
101. Sundararaman, R. et al. Theoretical predictions for hot-carrier generation from surface plasmon decay. *Nat. Commun.* **5**, 5788 (2014).
102. Mubeen, S., Lee, J., Liu, D., Stucky, G. D. & Moskovits, M. Panchromatic photoproduction of H_2 with surface plasmons. *Nano Lett.* **15**, 2132–2136 (2015).
103. Harutyunyan, H. et al. Anomalous ultrafast dynamics of hot plasmonic electrons in nanostructures with hot spots. *Nat. Nanotech.* **10**, 770–774 (2015).
104. Manjavacas, A., Liu, J. G., Kulkarni, V. & Nordlander, P. Plasmon-induced hot carriers in metallic nanoparticles. *ACS Nano* **8**, 7630–7638 (2014).
105. Haruta, M. Size- and support-dependency in the catalysis of gold. *Catal. Today* **36**, 153–166 (1997).
106. Furube, A., Du, L., Hara, K., Katoh, R. & Tachiya, M. Ultrafast plasmon-induced electron transfer from gold nanodots into TiO_2 nanoparticles. *J. Am. Chem. Soc.* **129**, 14852–14853 (2007).
107. Wu, K., Chen, J., McBride, J. R. & Lian, T. Efficient hot-electron transfer by a plasmon-induced interfacial charge-transfer transition. *Science* **349**, 632–635 (2015).
108. Zheng, B. Y. et al. Distinguishing between plasmon-induced and photoexcited carriers in a device geometry. *Nat. Commun.* **6**, 7797 (2015).
109. Li, J. et al. Plasmon-induced resonance energy transfer for solar energy conversion. *Nat. Photon.* **9**, 601–607 (2015).
110. Maher, R. C. et al. Stokes/anti-Stokes anomalies under surface enhanced Raman scattering conditions. *J. Chem. Phys.* **120**, 11746–11753 (2004).
111. Sushchinskii, M. M. & Rousseau, D. L. Raman spectra of molecules and crystals. *Phys. Today* **26**, 61–62 (2008).
112. Sun, M., Zhang, Z., Zheng, H. & Xu, H. In-situ plasmon-driven chemical reactions revealed by high vacuum tip-enhanced Raman spectroscopy. *Sci. Rep.* **2**, 647–650 (2012).
113. Zhang, Z. et al. Insights into the nature of plasmon-driven catalytic reactions revealed by HV-TERS. *Nanoscale* **5**, 3249–3252 (2013).
114. Haslett, T. L., Tay, L. & Moskovits, M. Can surface-enhanced Raman scattering serve as a channel for strong optical pumping? *J. Chem. Phys.* **113**, 1641–1646 (2000).
115. Brolo, A. G., Sanderson, A. C. & Smith, A. P. Ratio of the surface-enhanced anti-Stokes scattering to the surface-enhanced Stokes-Raman scattering for molecules adsorbed on a silver electrode. *Phys. Rev. B* **69**, 045424 (2004).
116. Maher, R. C. et al. Resonance contributions to anti-Stokes/Stokes ratios under surface enhanced Raman scattering conditions. *J. Chem. Phys.* **123**, 084702 (2005).
117. S., Y. Y. & Tamitake, I. Why and how do the shapes of surface-enhanced Raman scattering spectra change? Recent progress from mechanistic studies. *J. Raman Spectrosc.* **47**, 78–88 (2016).
118. Itoh, T. et al. Second enhancement in surface-enhanced resonance Raman scattering revealed by an analysis of anti-Stokes and Stokes Raman spectra. *Phys. Rev. B* **76**, 085405 (2007).
119. Li, J. F. et al. Shell-isolated nanoparticle-enhanced Raman spectroscopy. *Nature* **464**, 392–395 (2010).
120. Robatjazi, H. et al. Plasmon-induced selective carbon dioxide conversion on earth-abundant aluminum-cuprous oxide antenna-reactor nanoparticles. *Nat. Commun.* **8**, 27 (2017).
121. Aslam, U., Chavez, S. & Linic, S. Controlling energy flow in multimetallic nanostructures for plasmonic catalysis. *Nat. Nanotech.* **12**, 1000–1005 (2017).
122. Grigorenko, A. N., Polini, M. & Novoselov, K. S. Graphene plasmonics. *Nat. Photon.* **6**, 749–758 (2012).
123. Lalisse, A., Tessier, G., Plain, J. & Baffou, G. Quantifying the efficiency of plasmonic materials for near-field enhancement and photothermal conversion. *J. Phys. Chem. C* **119**, 25518–25528 (2015).
124. Voiry, D., Shin, H. S., Loh, K. P. & Chhowalla, M. Low-dimensional catalysts for hydrogen evolution and CO2 reduction. *Nat. Rev. Chem.* **2**, 0105 (2018).
125. Boltasseva, A. & Atwater, H. A. Low-loss plasmonic metamaterials. *Science* **331**, 290–291 (2011).
126. Cushing, S. K. et al. Photocatalytic activity enhanced by plasmonic resonant energy transfer from metal to semiconductor. *J. Am. Chem. Soc.* **134**, 15033–15041 (2012).
127. Chikkaraddy, R. et al. Single-molecule strong coupling at room temperature in plasmonic nanocavities. *Nature* **535**, 127–130 (2016).
128. Benz, F. et al. Single-molecule optomechanics in "picocavities". *Science* **354**, 726–729 (2016).
129. Schlather, A. E. et al. Hot hole photoelectrochemistry on Au@SiO2@Au nanoparticles. *J. Phys. Chem. Lett.* **8**, 2060–2067 (2017).
130. Zhu, W. et al. Quantum mechanical effects in plasmonic structures with subnanometre gaps. *Nat. Commun.* **7**, 11495 (2016).
131. Cortés, E. et al. Plasmonic hot electron transport drives nano-localized chemistry. *Nat. Commun.* **8**, 14880 (2017).
132. Wang, P., Krasavin, A. V., Nasir, M. E., Dickson, W. & Zayats, A. V. Reactive tunnel junctions in electrically driven plasmonic nanorod metamaterials. *Nat. Nanotech.* **13**, 159–164 (2018).
133. Kazuma, E., Jung, J., Ueba, H., Trenary, M. & Kim, Y. Real-space and real-time observation of a plasmon-induced chemical reaction of a single molecule. *Science* **360**, 521–526 (2018).
134. Zhang, Y. et al. Visualizing coherent intermolecular dipole-dipole coupling in real space. *Nature* **531**, 623–627 (2016).
135. Zhang, Y. et al. Sub-nanometre control of the coherent interaction between a single molecule and a plasmonic nanocavity. *Nat. Commun.* **8**, 15225 (2017).
136. Liu, X. & Swihart, M. T. Heavily-doped colloidal semiconductor and metal oxide nanocrystals: an emerging new class of plasmonic nanomaterials. *Chem. Soc. Rev.* **43**, 3908–3920 (2014).
137. V., N. G., M., S. V. & Alexandra, B. Alternative plasmonic materials: beyond gold and silver. *Adv. Mater.* **25**, 3264–3294 (2013).
138. Stensitzki, T. et al. Acceleration of a ground-state reaction by selective femtosecond-infrared-laser-pulse excitation. *Nat. Chem.* **10**, 126 (2018).
139. Petek, H. Photoexcitation of adsorbates on metal surfaces: one-step or three-step. *J. Chem. Phys.* **137**, 091704 (2012).

Acknowledgements
The authors are deeply grateful to M. Moskovits for his very helpful suggestions and careful academic and English editing of the manuscript. This work is financially supported by the National Natural Science Foundation of China (21533006, 21621091, 91427304 and 21403180) and the Ministry of Science and Technology of China (2015CB932300).

Author contributions
Z-Q.T. conceived the outline. C.Z., X-J.C. and Z-Q.T. wrote the manuscript. J.Y. supplied the calculation in Figure 1. All authors contributed to discussions, editing and corrections. C.Z. and Z-Q.T. revised the manuscript before the final submission.

Competing interests
The authors declare no competing interests.

Reviewers information
Nature *Reviews Chemistry* thanks R. Aroca, S. Schlücker and the other anonymous reviewer(s) for their contribution to the peer review of this work.